NANO LETTERS

Communication

Electrical charge state manipulation of single silicon vacancies in a silicon carbide quantum optoelectronic device

Matthias Widmann, Matthias Niethammer, Dmitry Yu Fedyanin, Igor A. Khramtsov, Torsten Rendler, Ian D. Booker, Jawad Ul Hassan, Naoya Morioka, Yu-Chen Chen, Ivan G. Ivanov, Nguyen Tien Son, Takeshi Ohshima, Michel Bockstedte, Adam Gali, Cristian Bonato, Sang-Yun Lee, and Jörg Wrachtrup

Nano Lett., **Just Accepted Manuscript** • DOI: 10.1021/acs.nanolett.9b02774 • Publication Date (Web): 18 Sep 2019

Electrical charge state manipulation of single silicon vacancies in a silicon carbide quantum optoelectronic device

Authors:

Matthias Widmann[1*], Matthias Niethammer[1], Dmitry Yu. Fedyanin[2], Igor A. Khramtsov[2], Torsten Rendler[1], Ian D. Booker[3], Jawad Ul Hassan[3], Naoya Morioka[1], Yu-Chen Chen[1], Ivan G. Ivanov[3], Nguyen Tien Son[3], Takeshi Ohshima[4], Michel Bockstedte[5,6], Adam Gali[7,8], Cristian Bonato[9], Sang-Yun Lee[1,10†] & Jörg Wrachtrup[1]

Affiliations:

[1] 3. Physikalisches Institut and Research Center SCOPE and Integrated Quantum Science and Technology (IQST), University of Stuttgart, Pfaffenwaldring 57, 70569 Stuttgart, Germany

[2] Laboratory of Nanooptics and Plasmonics, Moscow Institute of Physics and Technology, 9 Institutsky Lane, 141700 Dolgoprudny, Russian Federation

[3] Department of Physics, Chemistry and Biology, Linköping University, SE-58183 Linköping, Sweden

[4] National Institutes for Quantum and Radiological Science and Technology, Takasaki, Gunma 370-1292, Japan

[5] Department Chemistry and Physics of Materials, University of Salzburg, Jakob-Haringer-Str. 2a, 5020 Salzburg, Austria

[6] Solid State Theory, University of Erlangen-Nuremberg, Staudstr. 7B2, 91058 Erlangen, Germany

[7] Wigner Research Centre for Physics, Hungarian Academy of Sciences, PO. Box 49, H-1525 Budapest, Hungary

[8] Department of Atomic Physics, Budapest University of Technology and Economics, Budafoki út 8., H-1111 Budapest, Hungary

[9] Institute of Photonics and Quantum Sciences, SUPA, Heriot-Watt University, Edinburgh EH14 4AS, UK

[10] Center for Quantum Information, Korea Institute of Science and Technology, Seoul, 02792, Republic of Korea

*m.widmann@pi3.uni-stuttgart.de

†sangyun.lee236@gmail.com

Abstract

Color centers with long-lived spins are established platforms for quantum sensing and quantum information applications. Color centers exist in different charge states, each of them with distinct optical and spin properties. Application to quantum technology requires the capability to access and stabilize charge states for each specific task. Here, we investigate charge state manipulation of individual silicon vacancies in silicon carbide, a system which has recently shown a unique combination of long spin coherence time and ultrastable spin-selective optical transitions. In particular, we demonstrate charge state switching through the bias applied to the color center in an integrated silicon carbide opto-electronic device. We show that the electronic environment defined by the doping profile and the distribution of other defects in the device plays a key role for charge state control. Our experimental results and numerical modelling evidence that control of these complex interactions can, under certain conditions, enhance the photon emission rate. These findings open the way for deterministic control over the charge state of spin-active color centers for quantum technology and provide novel techniques for monitoring doping profiles and voltage sensing in microscopic devices.

Individual spins associated with quantum emitters in semiconductors are an established platform for quantum metrology and quantum information processing [1–5]. The possibility to manipulate individual spins builds on the capability to control the number of charges in a system, at the level of single electrons or single holes. This has been achieved with great success in the case of semiconductor quantum dots, through the Coulomb blockade effect [6–8]. Alternatively, color centers can provide a system where individual spins can be controlled and detected, even at room temperature. Color centers can exist in different charge states, each with a specific electronic structure featuring unique optical and spin properties. For example, the negative charge state of the nitrogen-vacancy (NV) center in diamond hosts a coherent electronic spin which can be polarized and readout optically [1]. These properties have been exploited for quantum sensing [9,10,2,3] with nanoscale spatial resolution [11] and for seminal demonstrations of quantum networking [12–14]. Techniques have been developed to stabilize the color center charge state [15–18], as its fluctuations due to either noisy environment in solids or applied electromagnetic fields for control and readout is responsible for inefficiency in various applications [19–21,22]. Undesired switching to a different charge state precludes interfacing the electronic spin to photons. The fidelity of spin-photon interfacing can be preserved by triggering the experiment to start only when the color center is in the required charge state [14,23]. This, however, reduces protocol efficiency, decreasing the overall quantum communication rate [14]. In some applications, the possibility to switch between different charge states can enable novel functionalities, such as protecting a nuclear spin quantum memory by converting the color center to a spin-less charge state [24,25]. In general, precise control the charge state of the spin-active color center enables selecting the optimal properties relevant for the specific task [26–29].

Electrical control, by the bias applied through an electronic device, is a convenient and potentially deterministic way to access and manipulate any available charge state of a color center [29,30]. However, this is difficult in insulators and many wide-bandgap semiconductors like diamond. In this respect, silicon carbide (SiC) is a promising alternative since it uniquely combines the availability of several different color centers featuring excellent quantum properties [30–35], with doping over a wide range of carrier densities [36,37], n-type as well as p-type. In addition, SiC features mature CMOS-compatible fabrication processes [38], which is a great benefit for scalable applications.

Recently, de las Casas et al. demonstrated charge state control of divacancies in SiC by biasing top gate electrodes. While such top-gate devices can be fabricated conveniently, only a limited area not covered by top gates can be optically accessed. In order to fabricate a device which has no limited optical access, we elucidate mature fabrication capability of SiC to prepare a p-i-n junction device. Highly doped, thin p- and n-type layers, sandwiching an intrinsic layer, enable optical access to color centers in the i-layer and electrical biasing as well. Because this type of device can also be used for electrical driving of color centers and improving efficiency of photoelectrical spin state readout, which is based on charge-state conversion and has been demonstrated in both diamond and SiC, it can be a basis for a multi-functional quantum device. In this work, we focus on the single silicon vacancy (V_{Si}) in 4H-SiC and demonstrate electrical switching between the negatively-charged ($V_{Si}^{(-)}$) and the neutral ($V_{Si}^{(0)}$) charge states. The $V_{Si}^{(-)}$ has recently gained attention for its long spin coherence times [32,35,39–41], a strong optically-detected spin signal at cryogenic temperature [42,43,44], and ultrastable spin-selective optical transitions [44,45]. This combination of properties make it an extremely promising system to demonstrate efficient spin-to-photon interfacing for quantum networking [1]. However, very little is known about how the V_{Si} charge state can be established and what the charge conversion mechanisms are. Here, we integrate single V_{Si} centers into the intrinsic region of a 4H-SiC p-i-n diode and experimentally demonstrate electrical switching of the charge state of a single V_{Si} by controlling the applied bias which appears as switching of the photon emission rate. In addition, enhancement of the photon emission is observed as well under specific applied bias values and optical excitation energies. To understand the microscopic nature of

the phenomena observed experimentally, we present and test a model which reveals a complex interplay between the quasi-Fermi level tuning and optical excitation of the vacancy and other nearby defects.

Charge state switching of the silicon vacancy

The SiC p-i-n diode structure (see Figure 1a,b) is grown by chemical vapour deposition (CVD) and consists of highly nitrogen-doped n-type and aluminum (Al)-doped p-type regions embedding a 50-µm-thick intrinsic layer. This intrinsic region is slightly p-type due to the residual Al and boron (B) impurities (see Supporting Information).

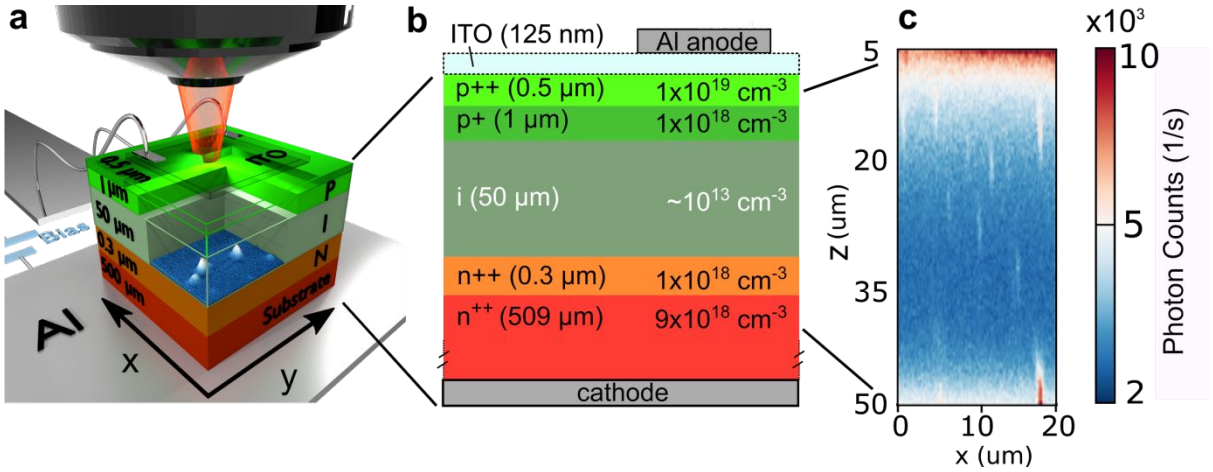

Figure 1. V_{Si} in SiC p-i-n junction device. (a) Schematic of the p-i-n diode structure. The metallic base plate is Al. Red and green layers are the heavily doped n- and p-type layer, respectively. The pastel green layer is the intrinsic region, which is slightly p-doped. The indium tin oxide (ITO) layer, which requires to form a transparent electrical contact, is on top of the p-type layer. (b) Detailed schematic of the device showing the thickness and the doping concentrations of each layer. (c) Room temperature confocal scan through the intrinsic layer.

In the first experiment, we perform a two-dimensional confocal scan of the device across the growth direction (z-axis) and one lateral axis (x-axis), at zero applied voltage (Figure 1c). Using optical excitation at a wavelength of 730 nm (1.70 eV), we find isolated emitters across the intrinsic layer, which are identified as silicon vacancies in the negatively-charged state ($V_{Si}^{(-)}$) at the cubic lattice site (k) (see Supporting Information). The optically detected spin Rabi oscillations of a single $V_{Si}^{(-)}$ as shown in Figure 2d (see Supporting Information) not only provide an evidence for $V_{Si}^{(-)}$ but also demonstrate that the capability of coherent spin manipulation and readout is maintained in the tested junction device. In the following we focus on the depletion region near the i-n junction of the diode structure. Strong band bending in this region gives the possibility to electrically control the charge states of the V_{Si} center simply when applying different bias voltages. We find that, while $V_{Si}^{(-)}$ in the intrinsic layer do not show significant changes in their density, the V_{Si} center near the i-n interface strongly respond to the applied bias: Figure 2a shows confocal raster scans of the same x-y plane near the i-n interface (which is at a depth of about 47 µm) under reverse, zero and forward biases. At the reverse bias, several emitters are turned on, while the forward bias turns off the emitters that are bright at zero bias. We attribute this to switching of the charge state of the V_{Si} from single negative to other dark charge states, which will be discussed in the subsequent sections.

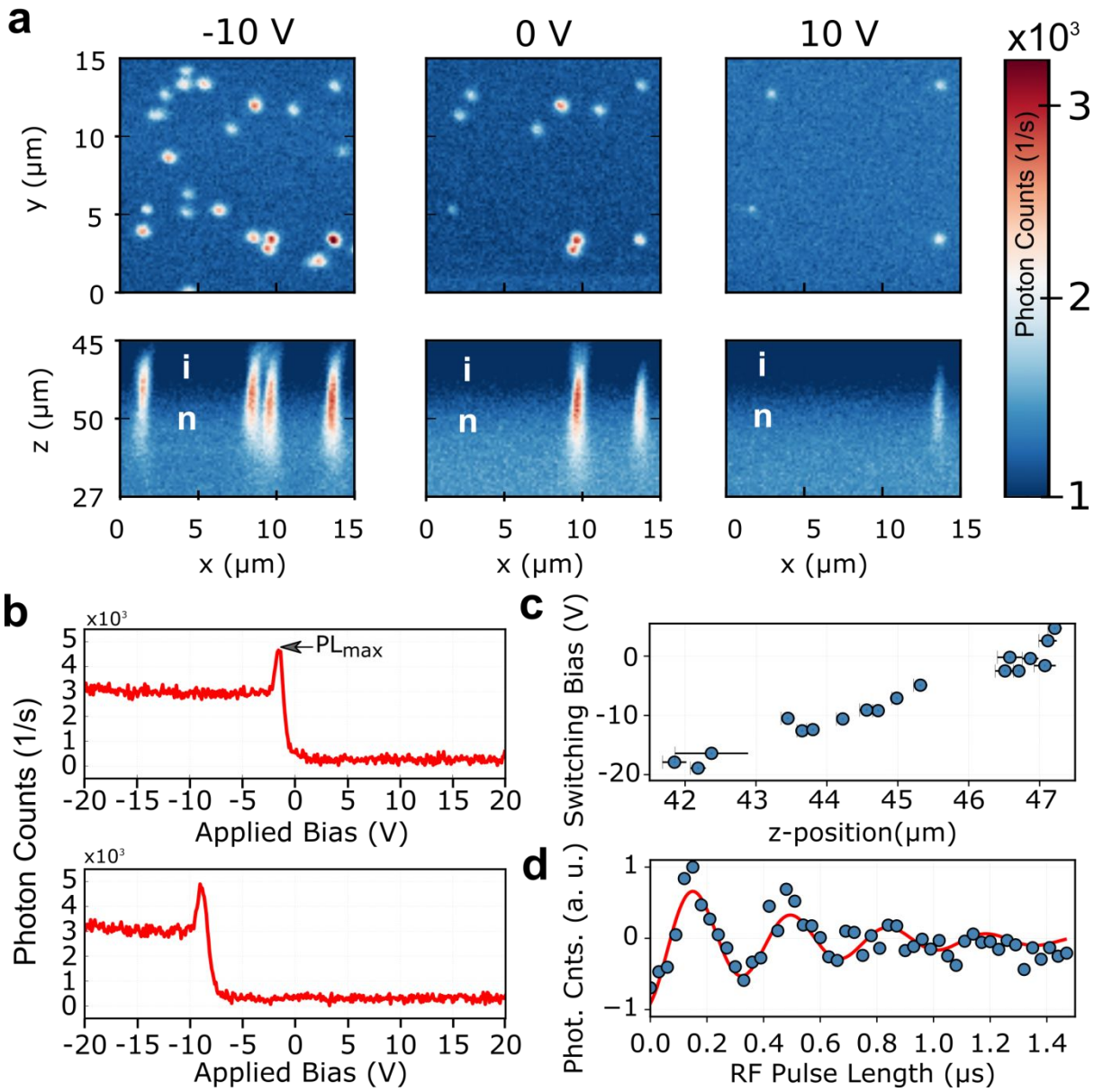

Figure 2. Electrical charge-state switching of single silicon vacancies. (a) Confocal scans at three bias voltages obtained at 1.5 mW (λ = 730 nm) optical excitation illustrating the charge state switching of V_{Si} centers near the i-n interface. The labels "i" and "n" indicate the intrinsic and n-type layers, respectively. (b) PL intensities of two selected single V_{Si} centers as a function of the bias voltage, illustrating the electrical switching of the charge states. (c) Dependence of the SB for individual V_{Si} centers on their position along the z-axis. Each circle indicates the position of the tested $V_{Si(-)}$ and the bias voltage at which the switching occurs. For every center, the SB is extracted from the PL intensity vs applied bias curve similar to that shown in panel (b). (d) Optically detected spin-Rabi oscillations of a single V_{Si} plotted at the expected resonant RF frequency. For (b) and (c), the optical excitation power is 5.5 mW (λ = 660 nm). See the text for details.

We also find that the newly switched-on emitters at reverse bias are located at a slightly further distance from the n-type layer. To test if the switching depends on the position of the V_{Si} center, we monitor the PL intensity of each bright emitter, while sweeping the bias voltage. Two selected results are shown in Figure 2b. The PL intensity is completely turned off at forward bias, while it is bright at reverse bias. A sharp increase in the PL intensity is observed at the bias value inducing the switching, namely the switching bias (SB). Figure 2b shows that the two tested emitters show different SB. To check if there

exists a relation between the SB and the emitter position, we perform several confocal z-scans around each emitter and find the exact z-position (see Supporting Information). By repeating this procedure on many emitters, we obtain a relation between the depth and the SB of each emitter as shown in Figure 2c. This plot demonstrates that a stronger reverse bias is necessary to switch on $V_{Si}^{(-)}$ emitters located farther from the i-n interface.

To test how optical excitation is related with the observations in Figure 1 and 2, we test 18 V_{Si} centers and monitor their PL intensity as a function of the applied voltage.

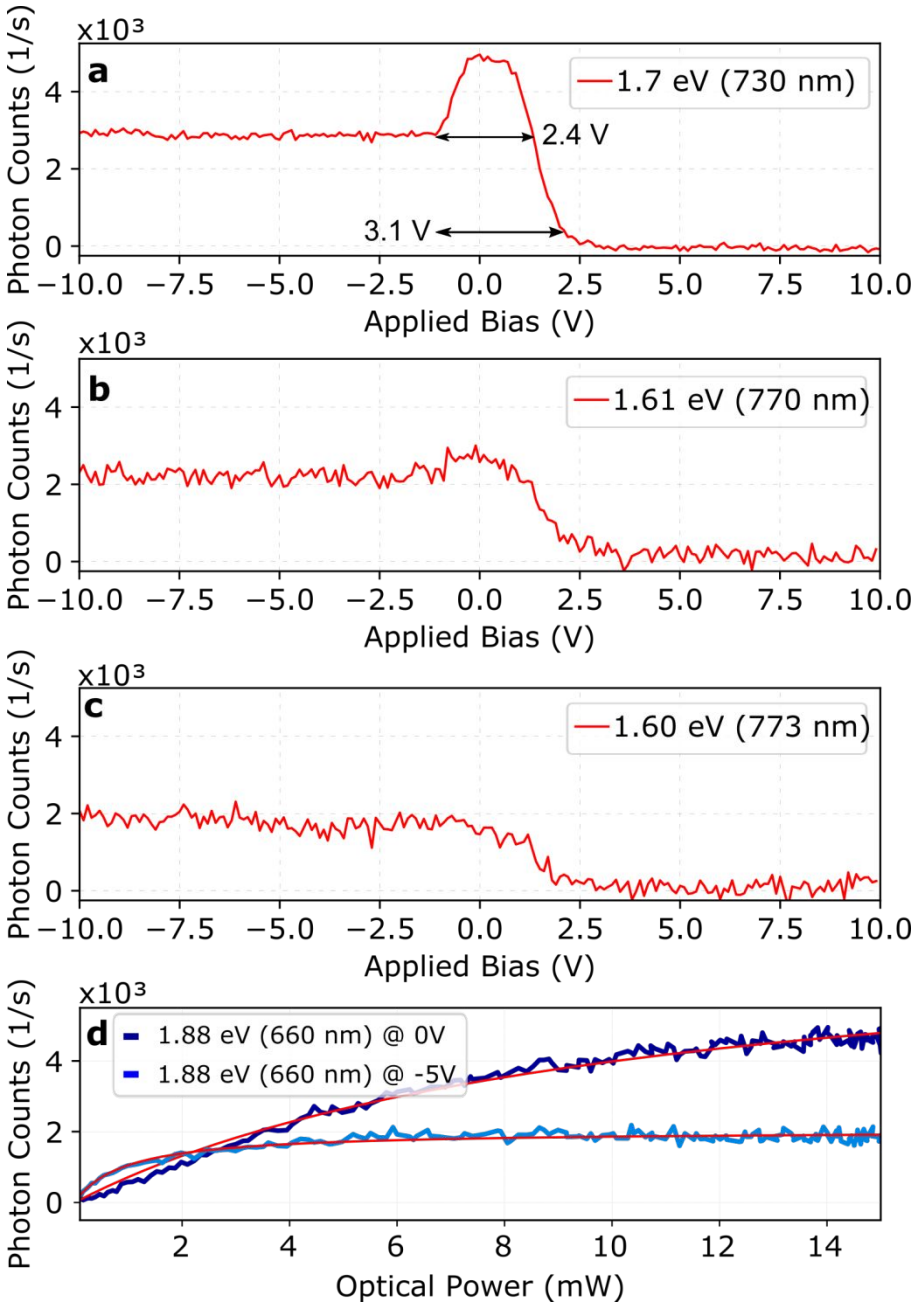

Figure 3. Optical excitation dependence of charge state conversion. (a-c) Bias dependent PL intensity curves under different excitation energies $\hbar\omega$: (a) 1.70 eV (730 nm), (b) 1.62 eV (765.5 nm), (c) 1.60 eV (773 nm). Arrows in a illustrate the width of increased PL (see text). (d) Optical saturation curves at 0 and -5 V, respectively, under 660 nm excitation. Solid lines

are fit using $I = \alpha P/(\beta + P)$, where α and β specify the saturated count rate and the saturation power which are fit parameters. At 0 V, α=5.2±0.3 kcts and β= 10±1 mW, and at -5V, α= 2.0±0.3 kcts and β = 0.90±0.01 mW.

In Figure 3a, the integrated PL intensity for the selected single V_{Si} near the i-n interface is plotted versus the bias voltage for $\hbar\omega$ = 1.7 eV (λ = 730 nm). Again, charge-state switching is observed at around 0 V together with a sharp peak in the PL intensity. To understand the origin of the enhanced PL intensity around the SB (≈0 V for the V_{Si} center in Figure 3), we vary the wavelength of the pump laser. Figure 3b shows that similar curves are obtained at $\hbar\omega > 1.60$ eV ($\lambda < 773$ nm). However, the peak in the PL intensity at the SB disappears at $\hbar\omega \lesssim 1.60$ eV ($\lambda \gtrsim 773$ nm) (Figure 3c) (see Figure S6). Figure 3d shows that the PL intensity under optical saturation is 2 times stronger at 0 V than that at -5 V. Other tested V_{Si} center show the same behaviour, except that the SB is different for each center. These results suggest that an optical excitation energy larger than 1.60 eV triggers an additional process, resulting in an abrupt increase of the PL intensity, in addition to the electrical charge state switching. In the following, we discuss underlying mechanisms for the observations above.

Charge states of the silicon vacancy

In thermal equilibrium, the occupation of the neutral (0), single (-1), double (-2) and triple (-3) charged states are determined by the position of the Fermi level with respect to the valence band edge.

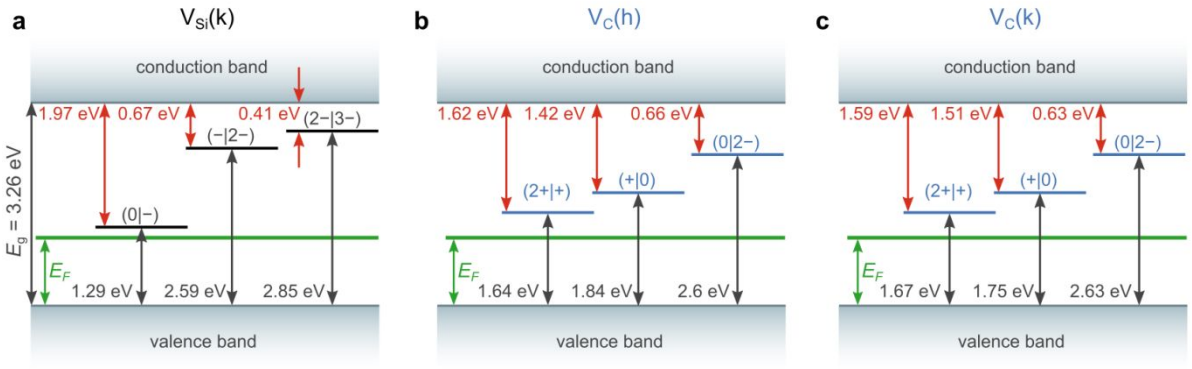

Figure 4. Charge states of the V_{Si} and V_C centers. Charge state transition levels of the (a) V_{Si} at the cubic lattice site and (b,c) V_C defects in 4H-SiC adopted from Refs. [26,46] . Note that we follow the recent assignment of the cubic and hexagonal defect of V_{Si} in Ref. [47]. Generic values are provided in panels (b) and (c). The green line schematically shows the Fermi level. The black (red) arrows indicate the optical ionization energy towards higher (lower) charged states.

The known transition levels among the charge states of the V_{Si}, which have a deep-acceptor nature, are depicted in Figure 4a. (see Supporting Information). Figure 5a shows the simulated energy band diagram of the fabricated p-i-n diode in equilibrium (see Supporting Information). In the p^{++}- and p^{+}-type layers and in most of the intrinsic layer, which is slightly p-type, the Fermi level is below the (0|-) transition level. Hence, in these regions, the V_{Si} is expected to be in the $V_{Si}^{(0)}$ state in equilibrium. However, under optical excitation, it may be ionized and converted into the $V_{Si}^{(-)}$ charge state. From the absorption spectrum of the $V_{Si}^{(0)}$ calculated using the CI-CRPA approach (see Supporting Information), we obtain an optical excitation threshold 0.9 eV (1380 nm) for the conversion of the $V_{Si}^{(0)}$ into the $V_{Si}^{(-)}$. Because the optical excitation energy in this work is larger than $\hbar\omega$ = 1.58 eV (785 nm), the $V_{Si}^{(-)}$ can be observed.

In the region near the i-n junction, in equilibrium, the Fermi level crosses all three charge state transition levels of the V_{Si} center (see Figure 5a). Hence, the V_{Si} center are expected to be in different charge states depending on their positions along the z-axis. For the charge state conversion in this region, we also have to take into account optical ionization. The conversion $V_{Si}^{(-)} \rightarrow V_{Si}^{(0)} + e^-$ is not likely since, it requires photon energy higher than 1.97 eV (629 nm), assuming only a single photon absorption process (see Figure 4a), whereas the highest energy used in this study is 1.8 eV. In addition, optical ionization of other defects located in the vicinity of the studied V_{Si} should also be considered, in particular, carbon vacancies (V_C), which are the most abundant intrinsic defects in 4H-SiC (Figure 4b,c). Due to optical ionization, excess electrons and holes are released from defects to the conduction and valence bands. These carriers can be captured by V_{Si} and other defects [48]. In our sample, the density of V_C is in the range from 5×10^{12} to 1×10^{13} cm^{-3} (see Supporting Information). Since this density corresponds to an average distance between V_C of ~300 nm, there is a good chance for a V_C to be located near the studied V_{Si}. This complexity is further increased by the non-equilibrium induced by the applied bias as we will discuss in the next sections.

Electrical control of the charge state

To explain the mechanism of electrical switching between the charge states of the V_{Si}, we self-consistently simulate the 4H-SiC p-i-n diode shown in Figure 1b (see Supporting Information). Figure 5b shows the simulated energy band diagram at a bias voltage of -15 V applied to the device, which corresponds to a voltage drop across the p-i-n diode of -3 V due to non-ideality of the fabricated device (see Supporting Information).

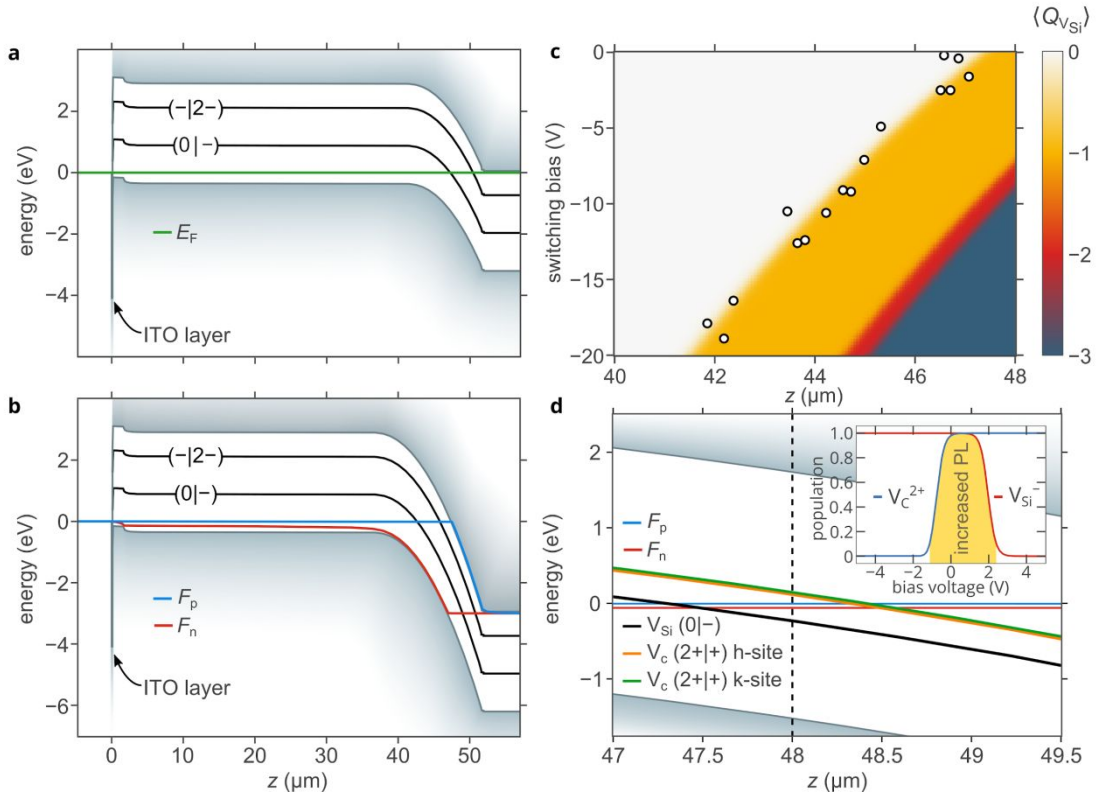

Figure 5. Charge state conversion by applied bias. (a,b) Simulated energy band diagrams of the fabricated device in thermal equilibrium (a) and at a reverse bias voltage of -15 V (b). Black solid lines show the positions of the charge transition levels (0|-) and (-|2-). The (2-|3-) transition level is not shown since it is located very close to the (-|2-) transition level. (c) Simulated evolution of the

spatial distribution of the time-averaged charge (i.e., averaged occupation of the neutral, (-1), (-2) and (-3) charge states as denoted by the color scale) of single silicon vacancies $<Q_{VSi}>$ with the reverse voltage applied to the device. Open dots represent the results of the experimental measurements shown in Figure 2c. (d) Energy band diagram at around z = 48 µm at V = -0.3 V. Inset: Populations of the (-1) charge state of the silicon vacancy and (+2) charge state of the carbon vacancy at z = 48.3 µm versus bias voltage. The yellow area shows the voltage range of the increased PL.

As the reverse bias increases, the band bending in the depletion region near the i-n junction increases and the depletion region expands towards the p-i junction. At the same time, the applied bias perturbs the carrier equilibrium , which splits the Fermi level E_F into two quasi-Fermi levels F_n and F_p for electrons and holes, respectively. Accordingly, the occupation of the charge states cannot be identified as easily as in equilibrium. One has to closely consider the processes of electron and hole capture and release by the V_{Si} in a manner similar to that used for the description of electroluminescence of color centers [34,49–51]. In the region where we observe switching of the charge state of the V_{Si} (see Figure 2c), we find that the density of holes is many orders of magnitude higher than that of electrons, even at significantly high voltages (seeFigure S9). In addition, there are no minority carriers in the reverse biased diode. Therefore, in the band bending region the occupation of the charge states of the V_{Si} is mainly determined by the hole capture and hole release processes. This situation is the same as in a p-type material in equilibrium. Thus, we can use the same expressions for the charge states populations of the V_{Si} as in equilibrium by replacing E_F with F_p. In other words, the transition between the charge states occurs when the quasi-Fermi level for holes crosses the corresponding transition level. Figure 5c shows the corresponding calculations based on this quasi-equilibrium approach, predicting electrical switching between the $V_{Si}^{(0)}$ and $V_{Si}^{(-)}$ states. According to calculations (see Supporting Information) , $V_{Si}^{(0)}$ is expected to emit in the near-infrared, with photon energies less than the ionization threshold (~0.9 eV). Emission, however, is expected to be weak due to competing non-radiative processes. Since the detectors used in the experiment are not sensitive for wavelengths larger than ~1000 nm, switching to the $V_{Si}^{(0)}$ charge state corresponds to a suppression of the PL signal. Together with these simulation results, the data in Figure 2b and Figure 3 show that the p-i-n diode structures allows to switch the charge state between $V_{Si}^{(0)}$ and $V_{Si}^{(-)}$ by applying a moderate voltage.

Reinitialization of the silicon vacancy

Finally, we turn to the origin of the increased PL at around the SB as shown in Figure 2b and Figure 3. For simplicity, we focus on the particular V_{Si} center located at a depth of about 48 µm, for which the measurements are shown in Figure 3. However, this analysis can be applied with no change to any observed V_{Si} in the studied 4H-SiC diode. As discussed in the previous section, around the SB voltage the occupation of the $V_{Si}^{(0)}$ steadily decreases from 100% to 0 and the occupation of the $V_{Si}^{(-)}$ increases from 0 to 100% as the bias voltage decreases (see Figure 3c). However, at optical excitation energies above 1.6 eV, we observe an increased PL rate in the voltage range from -1.1 V to 2.0 V (Figure 3a,b). This observation is confirmed by the PL spectra at 0 and -5 V which have identical shape but the total intensity at 0 V is larger (see Supporting Information). If the PL at voltages below -1.1 V corresponds to 100% occupation of the (-1) charge state, why does the PL rate at voltages between -1.1 V and 1.3 V become higher (see Figure 3a,b)? This is counterintuitive, since the occupation of the negative charge state (-1) cannot increase further. To resolve this contradiction and find an additional process that can trigger an increase in the PL intensity, we emphasize that the increased PL of the V_{Si} is accompanied with the charge state switching from (0) to (-1), and therefore we can expect that complex electron and hole capture and release processes may happen at around the SB. Additionally, the peak at the SB is observed only at optical excitation energies higher than 1.6 eV, which approximately coincides with the

optical ionization threshold of $V_C^{(2+)} \rightarrow V_C^{(+)}+h$ (Figure 4b,c). This suggests that, holes released by V_C under optical excitation may be captured by the $V_{Si}^{(-)}$.

To understand how V_C can affect the V_{Si} charge state, we simulate the energy band diagram in the vicinity of the V_{Si} at V = -0.3 V applied to the device (see Supporting Information), which corresponds to the voltage drop across the p-i-n diode of -0.06 V . Since at z = 48 μm, F_p lies above the V_{Si} (0|-) level, the considered V_{Si} is in the (-1) charge state. At the same time, at z=48 μm, F_p is below the V_C (2+|+) level. Accordingly, the V_C at z = 48 μm is in the (+2) charge state, so are all V_C defects at z < 48 μm. We assume a V_C in the vicinity of the V_{Si} can be ionized by the excitation laser, if $\hbar\omega \gtrsim 1.64$ eV (see Figure 4b,c), and release a hole to the valence band, i.e., $V_C^{(2+)} \rightarrow V_C^{(+)}+h$. This hole can be captured by the considered V_{Si}, thus $V_{Si}^{(-)}+h \rightarrow V_{Si}^{(0)}$. As an increased PL is evident, the $V_{Si}^{(0)}$ rapidly returns back into $V_{Si}^{(-)}$. There are two possibilities for this transition. (I) The excitation laser can ionize the $V_{Si}^{(0)}$, which is possible at photon energies 1.6-1.8 eV as shown in Figure S7), and bring the V_{Si} back to the $V_{Si}^{(-)}$ ground state. However, this cannot result in increased luminescence. (II) The $V_{Si}^{(0)}$ can capture an electron from the conduction band. This electron can be provided due to the non-ideality of the device, and consequently non-zero electron current, or by the photoionization of another defect located nearby the V_{Si}. The free electron is captured by the V_{Si} into the $V_{Si}^{(-)}$ excited state [34,49], which then relaxes to the $V_{Si}^{(-)}$ ground state via photon emission increasing the luminescence rate dramatically [34,49–51], thus, $V_{Si}^{(-)}$ is re-initialized. This mechanism explains the experimentally observed threshold optical energy of 1.6 eV and supports that the release of a hole by V_C ionization followed by its capture at the $V_{Si}^{(-)}$, which promotes the reinitialization of $V_{Si}^{(-)}$, is very likely. For a larger reverse bias, the band bending is steeper (see Figure 5b), so is the V_C (2+|+) level, which repeats the profile of the conduction and valence bands. Therefore, the point of intersection between the V_C (2+|+) level and F_p shifts toward the p-i interface. At V < -1.4 V, all carbon vacancies at $z \geq 48$ μm are in the (+1) charge state and consequently $V_C^{(2+)} \rightarrow V_C^{(+)}+h$ is not possible. This essentially stops the reinitialization of the $V_{Si}^{(-)}$. Thus, according to our theoretical model and numerical simulations, for the V_{Si} center at z = 48 μm, the enhanced PL should be observed in the voltage range from -1.4 to 1.5 V, which is in good agreement with the experimental values (from -1.1 to 2.0 V). Even better coincidence with the experimental results can be obtained assuming the V_{Si} to be at z = 48.3 μm (see inset in Figure 5d). In this case, the voltage range of the enhanced PL is from -1.1 to 2.4 V. Although the experimental observations can be qualitatively explained by our model, the proposed mechanism may not be the only explanation. Further understanding could be achieved by combining the method used in this study with other junction spectroscopic methods, such as deep level transient spectroscopy [52].

Conclusions

The results presented in this work show for the first time electrical manipulation of the charge states of single silicon vacancies centers in silicon carbide optoelectronic device. We demonstrate switching of the silicon vacancy in the i-region of the 4H-SiC p-i-n diode between the neutral and single negatively charged states. We also find that the optical ionization of the silicon vacancy and other nearby defects such as carbon vacancies play an important role in charge state switching. When the ionization of carbon vacancies re-initializes the silicon vacancy, we observe even an enhancement of the PL intensity of the silicon vacancy. Our work demonstrates not only a convenient way to control the charge state of atomic-scale defects in semiconductor quantum optoelectronic devices but also potential applications using the atomic-scale color centers as a probe for local Fermi levels. This may open a new pathway to design

efficient and robust quantum interfaces for quantum-repeater applications [44] and may improve efficiency of quantum internet protocols [14] since idling time in an unfavoured dark state can be minimized. The demonstrated method may be extended to other color centers in silicon carbide [1] and similar materials [53,54], and used as an atomic-scale probe to characterize the distributions of defects states at the junctions of optoelectronic devices. By further optimization of the device structure and doping, such as lateral p-i-n junction devices [55,56] , much steeper changes of the PL intensities at around the switching bias will lead to new methods to sense electrostatic potentials at the nanoscale.

Acknowledgement

The authors thank Brian Gerardot, Jaekwang Lee, Tsunenobu Kimoto, Helmut Fedder and Stefan Lasse for helpful discussions. This work is supported by the Ministry of Education and Science of the Russian Federation (8.9898.2017/6.7), the Russian Foundation for Basic Research (19-57-12008), grant of the President of the Russian Federation (MK-2602.2017.9), Baden-Württemberg Stiftung Programm: Internationale Spitzenforschung, the ERC SMel and the BMBF BRAINQSENS, the Korea Institute of Science and Technology institutional program (2E29580, 2E27110), the Swedish Research Council (VR 2016-04068 and VR 2016-05362), the Carl Tryggers Stiftelse för Vetenskaplig Forskning (CTS 15:339), the Swedish Energy Agency (43611-1), the Knut and Alice Wallenberg Foundation (KAW 2018.0071), the National Quantum Technology Program (Grant No. 2017-1.2.1-NKP-2017-00001), National Excellence Program (Grant No. KKP129866), and EU QuantERA Nanospin project (Grant No. 127902) from the National Office of Research, Development and Innovation in Hungary, and the Engineering and Physical Sciences Research Council (EP/P019803/1 and EP/S000550/1) and the Networked Quantum Information Technologies Hub (Oxford) and JSPS KAKENHI (17H01056 and 18H03770). Supercomputer time was granted on the HPC cluster of the RRZE of the Friedrich-Alexander Universität, Erlangen-Nürnberg, the Doppler-Cluster of the Paris-Lodron University Salzburg.

Supporting Information Available

Author Contributions

S-Y.L. conceived the conceptual idea; M.W. and S-Y.L. designed the charge state control experiment; S-Y.L. and N.T.S. designed the sample structure; M.W. performed the charge state control experiments; M.N., T.R., and S-Y.L. provided experimental assistance; J.U.H., I.G.I., and N.T.S. prepared the sample and characterized basic properties; T.O. performed electron irradiation; M.W., M.N., D.Y.F., I.A.K., N.M., C.B., and S-Y.L. analyzed the data; D.Y.F., and I.A.K. developed the theory and performed computations for charge state conversion; M.B. calculated the optical transitions of the studied defects; A.G. provided theoretical support; M.W., D.Y.F., M.B., C.B., N.M., T.R. and S-Y.L. wrote the manuscript; All authors discussed and commented on the manuscript.

REFERENCES

(1) Atatüre, M.; Englund, D.; Vamivakas, N.; Lee, S.-Y.; Wrachtrup, J. Material Platforms for Spin-Based Photonic Quantum Technologies. *Nat. Rev. Mater.* **2018**, *3* (5), 38–51.
(2) Casola, F.; van der Sar, T.; Yacoby, A. Probing Condensed Matter Physics with Magnetometry

Based on Nitrogen-Vacancy Centres in Diamond. *Nat. Rev. Mater.* **2018**, *3* (1), 17088.
(3) Degen, C. L.; Reinhard, F.; Cappellaro, P. Quantum Sensing. *Rev. Mod. Phys.* **2017**, *89* (3), 035002.
(4) Awschalom, D. D.; Hanson, R.; Wrachtrup, J.; Zhou, B. B. Quantum Technologies with Optically Interfaced Solid-State Spins. *Nature Photonics*. 2018, pp 516–527.
(5) Zwanenburg, F. A.; Dzurak, A. S.; Morello, A.; Simmons, M. Y.; Hollenberg, L. C. L.; Klimeck, G.; Rogge, S.; Coppersmith, S. N.; Eriksson, M. A. Silicon Quantum Electronics. *Reviews of Modern Physics*. 2013, 961–1019.
(6) Hanson, R.; Kouwenhoven, L. P.; Petta, J. R.; Tarucha, S.; Vandersypen, L. M. K. Spins in Few-Electron Quantum Dots. *Reviews of Modern Physics*. 2007, pp 1217–1265.
(7) Warburton, R. J. Single Spins in Self-Assembled Quantum Dots. *Nature Materials*. 2013, 483–493.
(8) Brotons-Gisbert, M.; Branny, A.; Kumar, S.; Picard, R.; Proux, R.; Gray, M.; Burch, K. S.; Watanabe, K.; Taniguchi, T.; Gerardot, B. D. Coulomb Blockade in an Atomically Thin Quantum Dot Coupled to a Tunable Fermi Reservoir. *Nat. Nanotechnol.* **2019**, *14* (5), 442.
(9) Balasubramanian, G.; Chan, I. Y.; Kolesov, R.; Al-Hmoud, M.; Tisler, J.; Shin, C.; Kim, C.; Wojcik, A.; Hemmer, P. R.; Krueger, A.; Hanke, T.; Leitenstorfer, A.; Bratschitsch, R.; Jelezko, F. Nanoscale Imaging Magnetometry with Diamond Spins under Ambient Conditions. *Nature* **2008**, *455* (7213), 648–651.
(10) Häberle, T.; Schmid-Lorch, D.; Karrai, K.; Reinhard, F.; Wrachtrup, J. High-Dynamic-Range Imaging of Nanoscale Magnetic Fields Using Optimal Control of a Single Qubit. *Phys. Rev. Lett.* **2013**, *111* (17), 170801.
(11) Hong, S.; Grinolds, M. S.; Pham, L. M.; Le Sage, D.; Luan, L.; Walsworth, R. L.; Yacoby, A. Nanoscale Magnetometry with NV Centers in Diamond. *MRS Bull.* **2013**, *38* (02), 155–161.
(12) Hensen, B.; Bernien, H.; Dréau, A. E.; Reiserer, A.; Kalb, N.; Blok, M. S.; Ruitenberg, J.; Vermeulen, R. F. L.; Schouten, R. N.; Abellán, C.; Amaya, W.; Pruneri, V.; Mitchell, M. W.; Markham, M.; Twitchen, D.J.; Elkouss, D.; Wehner, S.; Taminiau, T.H.; Hanson, R. Loophole-Free Bell Inequality Violation Using Electron Spins Separated by 1.3 Kilometres. *Nature* **2015**, *526* (7575), 682–686.
(13) Kalb, N.; Reiserer, A. A.; Humphreys, P. C.; Bakermans, J. J. W.; Kamerling, S. J.; Nickerson, N. H.; Benjamin, S. C.; Twitchen, D. J.; Markham, M.; Hanson, R. Entanglement Distillation between Solid-State Quantum Network Nodes. *Science* **2017**, *356* (6341), 928–932.
(14) Humphreys, P. C.; Kalb, N.; Morits, J. P. J.; Schouten, R. N.; Vermeulen, R. F. L.; Twitchen, D. J.; Markham, M.; Hanson, R. Deterministic Delivery of Remote Entanglement on a Quantum Network. *Nature* **2018**, *558* (7709), 268–273.
(15) Doi, Y.; Makino, T.; Kato, H.; Takeuchi, D.; Ogura, M.; Okushi, H.; Morishita, H.; Tashima, T.; Miwa, S.; Yamasaki, S.; Neumann, P.; Wrachtrup, J.; Suzuki, Y.; Mizuochi, N. Deterministic Electrical Charge-State Initialization of Single Nitrogen-Vacancy Center in Diamond. *Physical Review X* **2014**, *4* (1), 011057.
(16) Petráková, V.; Nesládek, M.; Taylor, A.; Fendrych, F.; Cígler, P.; Ledvina, M.; Vacík, J.; Štursa, J.; Kučka, J. Luminescence Properties of Engineered Nitrogen Vacancy Centers in a Close Surface Proximity. *physica status solidi (a)*. 2011, 2051–2056.
(17) Fávaro de Oliveira, F.; Antonov, D.; Wang, Y.; Neumann, P.; Momenzadeh, S. A.; Häußermann, T.; Pasquarelli, A.; Denisenko, A.; Wrachtrup, J. Tailoring Spin Defects in Diamond by Lattice Charging. *Nat. Commun.* **2017**, *8*, 15409.
(18) Grotz, B.; Hauf, M. V.; Dankerl, M.; Naydenov, B.; Pezzagna, S.; Meijer, J.; Jelezko, F.; Wrachtrup, J.; Stutzmann, M.; Reinhard, F.; Garrido, J. A. Charge State Manipulation of Qubits in Diamond. *Nat. Commun.* **2012**, *3*, 729.
(19) Bradac, C.; Gaebel, T.; Naidoo, N.; Sellars, M. J.; Twamley, J.; Brown, L. J.; Barnard, A. S.; Plakhotnik, T.; Zvyagin, A. V.; Rabeau, J. R. Observation and Control of Blinking Nitrogen-Vacancy Centres in Discrete Nanodiamonds. *Nat. Nanotechnol.* **2010**, *5* (5), 345–349.
(20) Han, K. Y.; Wildanger, D.; Rittweger, E.; Meijer, J.; Pezzagna, S.; Hell, S. W.; Eggeling, C. Dark State Photophysics of Nitrogen–vacancy Centres in Diamond. *New Journal of Physics*. 2012, 123002.
(21) Aslam, N.; Waldherr, G.; Neumann, P.; Jelezko, F.; Wrachtrup, J. Photo-Induced Ionization

Dynamics of the Nitrogen Vacancy Defect in Diamond Investigated by Single-Shot Charge State Detection. *New Journal of Physics*. 2013, 013064.
(22) Chu, Y.; de Leon, N. P.; Shields, B. J.; Hausmann, B.; Evans, R.; Togan, E.; Burek, M. J.; Markham, M.; Stacey, A.; Zibrov, A. S.; Yacoby, A.; Twitchen, D. J.; Loncar, M.; Park, H.; Maletinsky, P.; Lukin, M. D. Coherent Optical Transitions in Implanted Nitrogen Vacancy Centers. *Nano Letters*. 2014, 1982–1986.
(23) Waldherr, G.; Wang, Y.; Zaiser, S.; Jamali, M.; Schulte-Herbrüggen, T.; Abe, H.; Ohshima, T.; Isoya, J.; Du, J. F.; Neumann, P.; Wrachtrup, J. Quantum Error Correction in a Solid-State Hybrid Spin Register. *Nature*. 2014, 204–207.
(24) Saeedi, K.; Simmons, S.; Salvail, J. Z.; Dluhy, P.; Riemann, H.; Abrosimov, N. V.; Becker, P.; Pohl, H.-J.; Morton, J. J. L.; Thewalt, M. L. W. Room-Temperature Quantum Bit Storage Exceeding 39 Minutes Using Ionized Donors in Silicon-28. *Science* **2013**, *342* (6160), 830–833.
(25) Pfender, M.; Aslam, N.; Simon, P.; Antonov, D.; Thiering, G.; Burk, S.; Fávaro de Oliveira, F.; Denisenko, A.; Fedder, H.; Meijer, J.; Garrido, J. A.; Gali, A.; Teraji, T.; Isoya, J.; Doherty, M. W.; Alkauskas, A.; Gallo, A.; Grünsei, A.; Neumann, P.; Wrachtrup, J. Protecting a Diamond Quantum Memory by Charge State Control. *Nano Lett.* **2017**, *17* (10), 5931–5937.
(26) Szász, K.; Ivády, V.; Abrikosov, I. A.; Janzén, E.; Bockstedte, M.; Gali, A. Spin and Photophysics of Carbon-Antisite Vacancy Defect in 4H Silicon Carbide: A Potential Quantum Bit. *Phys. Rev. B* **2015**, *91* (12), 121201(R).
(27) Wolfowicz, G.; Anderson, C. P.; Yeats, A. L.; Whiteley, S. J.; Niklas, J.; Poluektov, O. G.; Heremans, F. J.; Awschalom, D. D. Optical Charge State Control of Spin Defects in 4H-SiC. *Nat. Commun.* **2017**, *8* (1), 1876.
(28) Dhomkar, S.; Henshaw, J.; Jayakumar, H.; Meriles, C. A. Long-Term Data Storage in Diamond. *Sci Adv* **2016**, *2* (10), 1600911.
(29) Broadway, D. A.; Dontschuk, N.; Tsai, A.; Lillie, S. E.; -K. Lew, C. T.; McCallum, J. C.; Johnson, B. C.; Doherty, M. W.; Stacey, A.; Hollenberg, L. C. L.; Tetienne, J. P. Spatial Mapping of Band Bending in Semiconductor Devices Using in Situ Quantum Sensors. *Nature Electronics* **2018**, *1* (9), 502.
(30) Casas, C. F. de las; de las Casas, C. F.; Christle, D. J.; Hassan, J. U.; Ohshima, T.; Son, N. T.; Awschalom, D. D. Stark Tuning and Electrical Charge State Control of Single Divacancies in Silicon Carbide. *Applied Physics Letters*. 2017, 262403.
(31) Christle, D. J.; Klimov, P. V.; de las Casas, C. F.; Szász, K.; Ivády, V.; Jokubavicius, V.; Hassan, J. U.; Syväjärvi, M.; Koehl, W. F.; Ohshima, T.; Son, N. T.; Janzén, E.; Gali, Á.; Awschalom, D. D. Isolated Spin Qubits in SiC with a High-Fidelity Infrared Spin-to-Photon Interface. *Phys. Rev. X* **2017**, *7* (2), 021046.
(32) Widmann, M.; Lee, S.-Y.; Rendler, T.; Son, N. T.; Fedder, H.; Paik, S.; Yang, L.-P.; Zhao, N.; Yang, S.; Booker, I.; Denisenko, A.; Jamali, M.; Momenzadeh, S. A., Gerhardt, I.; Ohshima, T.; Gali, Á.; Janzén, E.; Wrachtrup, J. Coherent Control of Single Spins in Silicon Carbide at Room Temperature. *Nat. Mater.* **2015**, *14* (2), 164–168.
(33) Castelletto, S.; Johnson, B. C.; Ivády, V.; Stavrias, N.; Umeda, T.; Gali, A.; Ohshima, T. A Silicon Carbide Room-Temperature Single-Photon Source. *Nat. Mater.* **2014**, *13* (2), 151–156.
(34) Khramtsov, I. A.; Vyshnevyy, A. A.; Fedyanin, D. Y. Enhancing the Brightness of Electrically Driven Single-Photon Sources Using Color Centers in Silicon Carbide. *npj Quantum Information* **2018**, *4* (1), 15.
(35) Simin, D.; Kraus, H.; Sperlich, A.; Ohshima, T.; Astakhov, G. V.; Dyakonov, V. Locking of Electron Spin Coherence above 20 Ms in Natural Silicon Carbide. *Physical Review B* **2017**, *95* (16), 161201.
(36) Evwaraye, A. O.; Smith, S. R.; Mitchel, W. C. Shallow and Deep Levels in N-type 4H-SiC. *J. Appl. Phys.* **1996**, *79* (10), 7726–7730.
(37) Stenger, I.; -A. Pinault-Thaury, M.; Kociniewski, T.; Lusson, A.; Chikoidze, E.; Jomard, F.; Dumont, Y.; Chevallier, J.; Barjon, J. Impurity-to-Band Activation Energy in Phosphorus Doped Diamond. *Journal of Applied Physics*. 2013, 073711.
(38) Dimitrijev, S. Silicon Carbide as a Material for Mainstream Electronics. *Microelectron. Eng.* **2006**, *83* (1), 123–125.
(39) Simin, D.; Fuchs, F.; Kraus, H.; Sperlich, A.; Baranov, P. G.; Astakhov, G. V.; Dyakonov, V.

High-Precision Angle-Resolved Magnetometry with Uniaxial Quantum Centers in Silicon Carbide. *Phys. Rev. Applied* **2015**, *4* (1), 014009.
(40) Niethammer, M.; Widmann, M.; Lee, S.-Y.; Stenberg, P.; Kordina, O.; Ohshima, T.; Son, N. T.; Janzén, E.; Wrachtrup, J. Vector Magnetometry Using Silicon Vacancies in 4H-SiC Under Ambient Conditions. *Phys. Rev. Applied* **2016**, *6* (3), 034001.
(41) Anisimov, A. N.; Simin, D.; Soltamov, V. A.; Lebedev, S. P.; Baranov, P. G.; Astakhov, G. V.; Dyakonov, V. Optical Thermometry Based on Level Anticrossing in Silicon Carbide. *Sci. Rep.* **2016**, *6*, 33301.
(42) Soltamov, V. A.; Soltamova, A. A.; Baranov, P. G.; Proskuryakov, I. I. Room Temperature Coherent Spin Alignment of Silicon Vacancies in 4H- and 6H-SiC. *Phys. Rev. Lett.* **2012**, *108* (22), 226402.
(43) Nagy, R.; Widmann, M.; Niethammer, M.; Dasari, D. B. R.; Gerhardt, I.; Soykal, Ö. O.; Radulaski, M.; Ohshima, T.; Vučković, J.; Son, N. T.; Ivanov, I. G.; Economou, S. E.; Bonato, C.; Lee, S. Y.; Wrachtrup, J. Quantum Properties of Dichroic Silicon Vacancies in Silicon Carbide. *Physical Review Applied* **2018**, *9* (3), 034022.
(44) Nagy, R.; Niethammer, M.; Widmann, M.; Chen, Y.-C.; Udvarhelyi, P.; Bonato, C.; Hassan, J. U.; Karhu, R.; Ivanov, I. G.; Son, N. T.; Maze, J. M.; Ohshima, T.; Soykal, Ö. O.; Gali, Á.; Lee, S. Y.; Kaiser, F.; Wrachtrup, J. High-Fidelity Spin and Optical Control of Single Silicon-Vacancy Centres in Silicon Carbide. *Nat. Commun.* **2019**, *10* (1), 1954.
(45) Banks, H. B.; Soykal, Ö. O.; Myers-Ward, R. L.; Kurt Gaskill, D.; Reinecke, T. L.; Carter, S. G. Resonant Optical Spin Initialization and Readout of Single Silicon Vacancies in 4H-SiC. *Phys. Rev. Applied* **2019**, *11* (2), 024013.
(46) Magnusson, B.; Son, N. T.; Csóré, A.; Gällström, A.; Ohshima, T.; Gali, A.; Ivanov, I. G. Excitation Properties of the Divacancy in 4H-SiC. *Phys. Rev. B Condens. Matter* **2018**, *98* (19), 195202.
(47) Ivády, V.; Davidsson, J.; Son, N. T.; Ohshima, T.; Abrikosov, I. A.; Gali, A. Identification of Si-Vacancy Related Room-Temperature Qubits in 4H Silicon Carbide. *Phys. Rev. B* **2017**, *96* (16), 161114.
(48) Trinh, X. T.; Szász, K.; Hornos, T.; Kawahara, K.; Suda, J.; Kimoto, T.; Gali, A.; Janzén, E.; Son, N. T. Negative-U Carbon Vacancy in 4H-SiC: Assessment of Charge Correction Schemes and Identification of the Negative Carbon Vacancy at the Quasicubic Site. *Phys. Rev. B* **2013**, *88* (23), 235209.
(49) Fedyanin, D. Y.; Agio, M. Ultrabright Single-Photon Source on Diamond with Electrical Pumping at Room and High Temperatures. *New J. Phys.* **2016**, *18* (7), 073012.
(50) Khramtsov, I. A.; Agio, M.; Fedyanin, D. Y. Dynamics of Single-Photon Emission from Electrically Pumped Color Centers. *Phys. Rev. Applied* **2017**, *8* (2), 024031.
(51) Khramtsov, I. A.; Agio, M.; Yu. Fedyanin, D. Kinetics of Single-Photon Emission from Electrically Pumped NV Centers in Diamond. *AIP Conf. Proc.* **2017**, *1874*, 040014.
(52) Booker, I. D.; Janzén, E.; Son, N. T.; Hassan, J.; Stenberg, P.; Sveinbjörnsson, E. Ö. Donor and Double-Donor Transitions of the Carbon Vacancy Related EH6/7 Deep Level in 4H-SiC. *J. Appl. Phys.* **2016**, *119* (23), 235703.
(53) Morfa, A. J.; Gibson, B. C.; Karg, M.; Karle, T. J.; Greentree, A. D.; Mulvaney, P.; Tomljenovic-Hanic, S. Single-Photon Emission and Quantum Characterization of Zinc Oxide Defects. *Nano Letters*. 2012, 949–954.
(54) Berhane, A. M.; Jeong, K.-Y.; Bodrog, Z.; Fiedler, S.; Schröder, T.; Triviño, N. V.; Palacios, T.; Gali, A.; Toth, M.; Englund, D.; Aharonovich, I. Single-Photon Emission: Bright Room-Temperature Single-Photon Emission from Defects in Gallium Nitride (Adv. Mater. 12/2017). *Advanced Materials*. 2017.
(55) Widmann, M.; Niethammer, M.; Makino, T.; Rendler, T.; Lasse, S.; Ohshima, T.; Hassan, J. U.; Son, N. T.; Lee, S.-Y.; Wrachtrup, J. Bright Single Photon Sources in Lateral Silicon Carbide Light Emitting Diodes. *Applied Physics Letters*. 2018, 231103.
(56) Sato, S.-I.; Honda, T.; Makino, T.; Hijikata, Y.; Lee, S.-Y.; Ohshima, T. Room Temperature Electrical Control of Single Photon Sources at 4H-SiC Surface. *ACS Photonics*. 2018, 3159–3165.